Korean J. Chem. Eng., 34(2), 366-375 (2017)
DOI: 10.1007/s11814-016-0266-4

pISSN: 0256-1115
eISSN: 1975-7220

Carbonization and CO_2 activation of scrap tires: Optimization of specific surface area by the Taguchi method

Zakaria Loloie, Mehrdad Mozaffarian†, Mansooreh Soleimani, and Neda Asassian

Department of Chemical Engineering, Amirkabir University of Technology, No. 424, Hafez Ave, P. O. Box 15875-4413, Tehran, Iran

(*Received 20 December 2015 • accepted 22 September 2016*)

Abstract−This research demonstrates the production of activated carbon from scrap tires via physical activation with carbon dioxide. A newly constructed apparatus was utilized for uninterrupted carbonization and activation processes. Taguchi experimental design (L16) was applied to conduct the experiments at different levels by altering six operating parameters. Carbonization temperature (550-700 °C), activation temperature (800-950 °C), process duration (30-120 min), CO_2 flow rate (400 and 600 cc/min) and heating rate (5 and 10 °C/min) were the variables examined in this study. The effect of parameters on the specific surface area (SSA) of activated carbon was studied, and the influential parameters were identified employing analysis of variance (ANOVA). The optimum conditions for maximum SSA were: carbonization temperature=650 °C, carbonization time=60 min, heating rate=5 °C/min, activation temperature=900 °C, activation time=60 min and CO_2 flow rate=400 cc/min. The most effective parameter was activation temperature with an estimated impact of 49%. The activated carbon produced under optimum conditions was characterized by pore and surface structure analysis, iodine adsorption test, ash content, scanning electron microscopy (SEM) and Fourier transform infrared spectroscopy (FTIR). The process yield for optimized activated carbon was 13.2% with the following properties: specific surface area=437 m^2/g, total pore volume=0.353 cc/g, iodine number=404.7 mg/g and ash content=13.9% along with an amorphous structure and a lot of oxygen functional groups. These properties are comparable to those of commercial activated carbons.

Keywords: Scrap Tires, Activated Carbon, Physical Activation, Taguchi, Specific Surface Area, Optimization

INTRODUCTION

Tires belong to a class of polymer compounds called thermoset polymers. They consist of three main constituents: (I) rubber (about 60 wt%), (II) carbon black (about 25-35 wt%), and (III) such additives as fillers and accelerators. Most of the transportation vehicle tires, *e.g.* butyl rubber (BR) and stirene-butadiene copolymer (SBR) [1], are a blend of natural (NR) and synthetic rubber (SR). A tire is typically made up of 85% hydrocarbon, 10-15% iron (in the form of bead wire and steel belts), and the rest (if any) could include textile components for reinforcement, and a variety of chemical ingredients [2]. It has been estimated that each year 1.5 billion tires are manufactured around the world, and 4 billion scrap tires end up in worldwide landfills and (scrap tire piles [3,4]. The tires are designed to withstand extreme conditions, to wit: moisture, light, ozone, and harsh mechanical stress. Complicated manufacturing processes and advanced constitutive components of tires have allowed a typical tire to remain in the environment for almost 100 years. Therefore, disposing used tires in landfills neither a wise nor sustainable solution [1].

Most countries attempt to recover the energy or the material from scrap tires. Some of them, like European Union members, have outlawed the dumping of scrap tires in landfills [5]. Scrap tires are widely put to use as tire derived fuel (TDF) in many industries like cement kilns, power plants, pulp and paper mills, and electrical utilities, where they face, more or less, the least environmental and legal requirements [1,6]. Aside from providing a good opportunity for reducing petroleum-based solid waste, TDF is also a suitable replacement for non-renewable fuels with high calorific value [7]. Making use of TDF in cement kilns will lower the manufacturing costs [8]; this practice, however, gives rise to the emission of dangerous sulfuric gases, in particular SO_x, which pose serious air pollution problems [9]. Another viable alternative for recycling of used tires is material restoration. Such fields as concrete and asphalt manufacturing, retreading, sport surfacing, noise barriers, and roofing applications are now taking advantage of scrap tire components in their products [10-13].

Char and activated carbon are obtained as bi-products of used tire material recovery, and a fair amount of research has been conducted on their preparation and characterization in recent years [14-21]. Activated carbon can be produced by a variety of raw material sources including agricultural scraps such as almond shell/olive stone/coconut shell, Eucalyptus and Wattle wood [22], brewer's yeast [23], sugarcane bagasse [24], as well as industrial scraps like paper mill sludge [25], plastics, fertilizers and tire scraps [26-29]. Used tires are one of the most popular raw materials for activated carbon production thanks to their high carbon content and their widespread availability from landfills [17]. Activated carbon is a porous adsorbent with a large surface area, which makes it appli-

†To whom correspondence should be addressed.
E-mail: mozaffarian@aut.ac.ir

cable to the separation processes involving gas and liquid phases. Activated carbon derived from used tires has also served as adsorbent for removal of dyes [30,31], phenol [32], copper [33], lead [34], mercury [35], Rhodamine B [36], Uranium (VI) [37] and pesticides [38] from solutions. It has also been utilized for NO_2 elimination [39], natural gas storage, and air pollution control [40]. In addition, liquid-phase adsorption especially in water and waste water treatment technologies has become quite established, and activated carbon is one of the early adsorbents used for this process due to its ease of manufacturing, abundance, and cheapness [41]. In fact, it was the primary adsorbent and has been known as the most prevailing one for water and waste water recycling purposes since 1940 [42]. There is a wide range of different organic and inorganic pollutants that can be removed from water and waste water through adsorption processes [43]. Considerable improvements have been achieved in the last decade towards manufacturing of activated carbon enjoying enhanced adsorption capacity [44].

The most common approaches to activate scrap tires and other raw materials are to apply chemical or physical activation techniques. Physical activation by carbon dioxide or steam is more prevalent than chemical activation as long as industrial processes are concerned. A thermal pyrolysis stage is usually carried out at relatively low temperatures (400-700 °C), and the activation stage is, in turn, applied at high temperatures (800-1,000 °C). Activation technique (physical or chemical), activating agent, and temperature have a direct bearing on activated carbon properties, to wit: surface area, pore volume and functional groups [17].

In this study, activated carbon was prepared from used tires and a physical activation process was performed with the aid of carbon dioxide as the activating agent. The proper adjustment of operating parameters, namely temperature, holding time, heating rate, and gas flow rate, is extremely crucial in order to produce a high quality activated carbon with high surface area and large pore volume. An Experimental design was implemented as a systematic method to optimize the operating parameters with the objective of maximizing the selected features of the product. The Taguchi design is an orthogonal array method that significantly reduces the number of experimental configurations and provides an independent evaluation of factors through a small number of trials [45].

Surface area is one of the predominant characteristics of every adsorbent including activated carbon. The other attributes of activated carbon such as adsorption power and pore volume have a direct relationship with surface area [46]. In this regard, the operating parameters were optimized to produce an activated carbon with the maximum specific surface area (SSA) adopting Taguchi method. Moreover, a fast activation process was applied in the activation stage immediately after the carbonization stage. To lower energy consumption and process time, no further activities like acid washing were performed following the activation stage. Other concepts discussed include the size of the reactor and altering the type of stainless steel for the reactor construction. The system was left to cool slowly for one night.

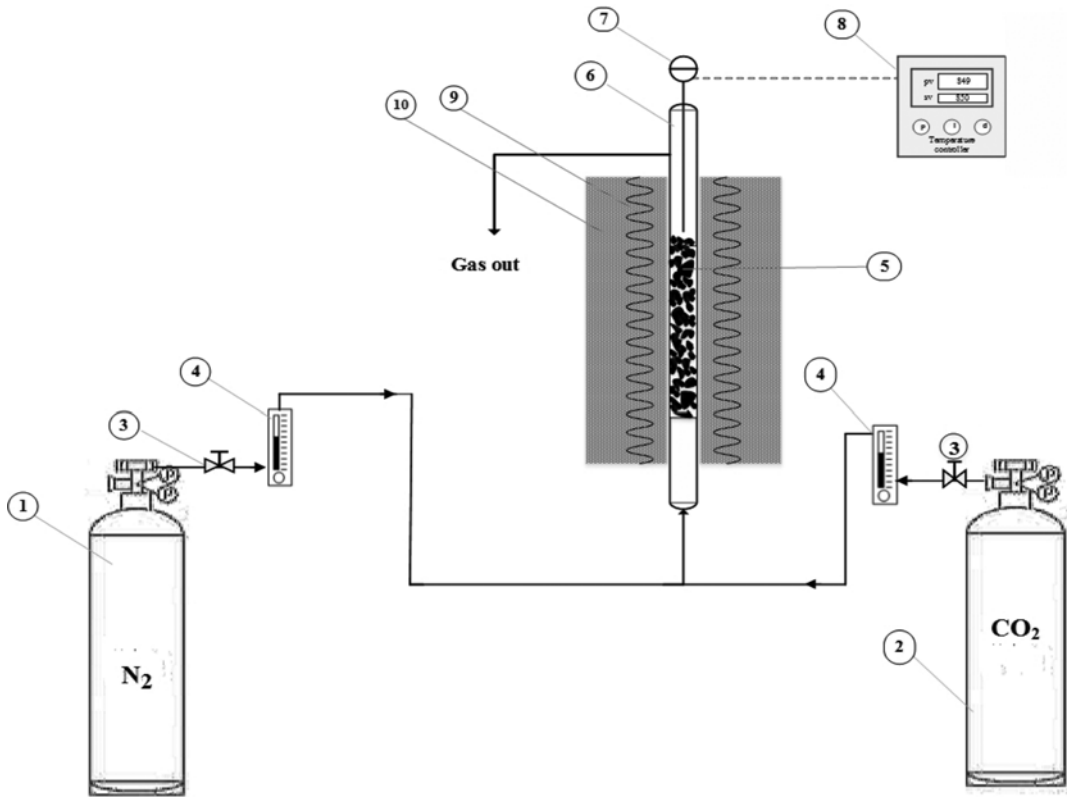

Fig. 1. Schematic display of experimental equipment set-up for activated carbon production from scrap tires.

1. Nitrogen cylinder
2. Carbon dioxide cylinder
3. Valve
4. Flowmeter
5. Scrap tires/activated carbon
6. Fixed bed reactor
7. Thermocouple
8. Temperature controller
9. Heating elements
10. Isolator

EXPERIMENTAL

1. Materials and Methods

Scrap tires were first crushed and shredded by an ambient crushing technology, and then sieved so that a stack of small particles with an average diameter of 3.5 mm was obtained. The particles containing steel and wire cords were removed with a powerful magnet. The particles also had 1% (w/w) of fiber cottons (nylon, rayon or polyester).

A fixed bed reactor was used to conduct the entire carbonization and activation processes, with the activation step run immediately after carbonization (Fig. 1). The tubular stainless steel reactor was ½ inch wide NPS and 1.1 m long. 50 grams of scrap tire particles were placed in the reactor, and nitrogen gas with a 99.99% purity and a flow rate of 100 cc/min was passed through the reactor for 15 minutes to completely purge the air from the reaction environment, and allow the pyrolysis process to proceed in the absence of oxygen. The electrical furnace was then turned on, and the temperature was elevated at a constant heating rate (°C/min) until the final carbonization temperature was reached. Eventually, the system was maintained at the carbonization temperature for a specific period of time called carbonization time.

At the end of carbonization process, the nitrogen flow was replaced by carbon dioxide so that the activation step could be initiated, while the furnace was simultaneously being heated to the final activation temperature at a constant heating rate. The system was kept at the activation temperature for a specific duration called activation time similar to the carbonization process. Finally, the system was cooled to room temperature for 24 hours, and the activated carbon was removed from the reactor. The yield of activated carbon production was calculated as follows:

$$\text{Yield}\ (\%) = \frac{W_2}{W_1} \times 100 \quad (1)$$

where W_1 is the initial weight of scrap tires (g), and W_2 is the weight of the obtained activated carbon (g).

2. Design of Experiments

Experimental design is a powerful approach for the optimization of parameters to get dependable results, and Taguchi method is one of the most tried-and-true, fastest techniques for design of experiments and response optimization. It is considered as a useful tool in many research studies and industrial R&D for product optimization. Quality control and enhancement of products, consistent products unaffected by fluctuations induced through undesirable environmental factors and components, saving time, energy, and material as well as significant reduction of costs are among the benefits of adopting Taguchi method [45].

We applied the Taguchi method to investigate the effect of all the important parameters associated with the activated carbon production process. Carbonization temperature, carbonization time, heating rate, activation temperature, activation time, and CO_2 gas flow rate were the selected operating parameters that could mainly influence the target response. The levels of operating parameters and their values are listed in Table 1.

Given Taguchi approach, an orthogonal array with six columns

Table 1. Operating parameters and their levels in activated carbon production

Parameter	Level 1	Level 2	Level 3	Level 4
Carbonization temperature (°C)	550	600	650	700
Carbonization time (min)	30	60	90	120
Heating rate (°C/min)	5	10	-	-
Activation temperature (°C)	800	850	900	950
Activation time (min)	30	60	90	120
CO_2 flow rate (cc/min)	400	600	-	-

Table 2. Orthogonal array (L16) of Taguchi experimental design

Run	parameters					
	Carbonization temp. (°C)	Carbonization time (min)	Heating rate (°C/min)	Activation temp. (°C)	Activation time (min)	CO_2 flow rate (cc/min)
C1	550	30	5	800	30	400
C2	550	60	5	850	60	600
C3	550	90	10	900	90	400
C4	550	120	10	950	120	600
C5	600	30	5	950	90	600
C6	600	60	5	900	120	400
C7	600	90	10	850	30	600
C8	600	120	10	800	60	400
C9	650	30	10	850	120	400
C10	650	60	10	800	90	600
C11	650	90	5	950	60	400
C12	650	120	5	900	30	600
C13	700	30	10	900	60	600
C14	700	60	10	950	30	400
C15	700	90	5	800	120	600
C16	700	120	5	850	90	400

and sixteen rows (L16) was sufficient for these experiments. The experimental L16 orthogonal array chart for these variables is presented in Table 2. To eliminate the noise effects of the factors, all the experiments were performed twice at the same operating conditions in a random way.

Surface area is one of the most important properties of activated carbon, and has a close correlation with other properties such as adsorption capacity, pore volume and pore width. In this research, the specific surface area (SSA), determined by employing the BET (Brunauer-Emmett-Teller) method, was taken as target response on which the process optimization was based. [47].

CHARACTERIZATION OF ACTIVATED CARBON

To characterize the synthesized activated carbon, the samples were specified by the following main physical and chemical properties:

1. Elemental Analysis

The compositions of raw material (tires) and final activated carbon were obtained via a Costech 4010 elemental analyzer. The relative amounts of the four elements including carbon, hydrogen, nitrogen and sulfur in the samples were reported as weight percent (wt%).

2. Surface Area and Pore Structure

The textural properties of the produced activated carbon were determined by nitrogen adsorption-desorption isotherm at 77 K. The isotherms were measured with a NOVA 1000 Quantachrome analyzer. All samples were degassed in a vacuum medium at 523 K for 3 hr before analysis. The Brunauer-Emmett-Teller (BET) equation was used to calculate the SSA with respect to a nitrogen molecule surface area of 0.162 nm^2 [47]. The total pore volumes and micropore volumes of the samples were calculated by the Dubinin-Radushkevich (DR) equation. The pore size distribution was evaluated by the Barrett-Joyner-Halenda (BJH) method [48].

3. Iodine Adsorption

Iodine number may serve as a criterion for adsorption capacity of carbon as well as its microporosity [49]; it indicates the amount of iodine (mg) adsorbed by 1 g of activated carbon. The iodine number of synthesized activated carbon was determined by titration as per the ASTM D4607-94 standard at 30 °C. About 2-3 g of each produced sample was taken, and fully wetted by 10 ml of 5 wt% HCl solution in a flask. Then, 100 ml of 0.1 N standard iodine solution was added to the flask, and the mixture was shaken vigorously for 1 minute. The mixture was then filtered and 50 ml of the filtered solution was quickly titrated with standard sodium thiosulfate (0.1 N) in the presence of starch as an indicator. Lastly, the iodine number was calculated from the total volume of consumed sodium thiosulfate.

4. Bulk Density

Bulk or apparent density is defined as a measure of the weight of material that a given volume can contain at specified conditions. A 10 ml cylinder was filled up to a certain volume with activated carbon that had been dried in an oven for 2 hr at 90 °C [50]. The cylinder was weighed and the bulk density was found by the following relation:

$$\text{Bulk density (g/ml)} = [\text{weight of activated carbon (g)} / \text{volume of packed dry activated carbon (ml)}] \quad (2)$$

5. pH

The pH test was done by means of a modified ASTM 3838-80 standard method [51]; so, 1 g of activated carbon was taken (instead of 10 g) while the carbon to water ratio was kept constant. A flask with a condenser was used to boil the sample in 10 ml of distilled water for 15 minutes. Then, the solution was filtered, and the pH of the filtrate was measured at 50 °C.

6. Ash Content

Based on the ASTM D2866 standard test method, the ash content was estimated in terms of the mass residue left after the carbon combustion. The sample was dried at 110 °C, and then moved to a muffle furnace where it was burned for 5 hr at 650 °C [52].

7. Conductivity

Conductivity was measured through the procedure suggested by Ahmenda [53]. A 1 wt% solution of activated carbon in deionized water was stirred at room temperature for 20 minutes. Afterwards, the electrical conductivity was measured using a WTWTCON 3110 conductivity meter.

8. FTIR

To identify the functional groups of the synthesized activated carbon, FTIR analysis was carried out by a Thermo Nicolet Nexus 670 spectrophotometer. The samples were mixed with KBr powder, and compressed into the disc by a manual tablet press, and then the FTIR analysis was accomplished in the absorbance mode.

9. Scanning Electron Microscopy (SEM)

Scanning electron microscopy (SEM) images were obtained with the help of the SERON AIS2300 microscope. The samples were powdered and dried in an oven at 110 °C before analysis.

RESULTS AND DISCUSSION

The carbon produced after carbonization of tire scraps (char) is ready to be activated by an activating agent like CO_2. The carbon atoms can be removed from the porous carbonaceous media through gasification using the activating agent (CO_2) at above 800 °C. The reaction of carbon with carbon dioxide is simple and defined as:

$$C + CO_2 \rightarrow 2\,CO \qquad \Delta H = +159\ \text{kJ/mol} \quad (3)$$

The resulting products of this reaction are carbon monoxide and porous activated carbon [46].

Table 3 shows the results for each run: process yield, textural properties of activated carbon, and ash content. The yield results range between 3 to 32%. These data indicate that the activated carbon yield was mostly influenced by temperature and holding time. As a result, the yields decreased substantially at high temperatures and relatively long holding times.

The ash content of activated carbon is deeply dependent on the mineral and/or inorganic compounds of the raw material. It consists mainly of alkali metal salts, silica, carbonates, etc., which is generally high in case of tire activated carbon due to the polymeric nature of rubber and the presence of other compounds in the tire structure such as oils and fillers. Commercial activated carbons have an ash content of up to 20%. Since ash occupies some of the pore volume and slows down the adsorption process, activated carbon with the least ash content is desired. There are some options, for instance, demineralization with HCl, to lessen the ash content. Con-

Table 3. Summary of results for activated carbon samples based on Taguchi experiments

Run	Yield (%)	Specific surface area (SSA)	Total pore volume ($\times 10^{-3}$ cc/g)	*t*-Method micropore volume ($\times 10^{-3}$ cc/g)	*t*-Method micropore surface area (m^2/g)	DR micropore volume ($\times 10^{-3}$ cc/g)	Ash (%)	Ave. pore radius (Å)
C1	32	93.75	113.7	7.6	11.4	61.2	11.6	24.3
C2	25	260.07	274.4	65.1	121.4	135.5	10.1	22.8
C3	15	366.84	333.7	112.2	176.3	179.0	6.9	18.9
C4	3	19.55	23.4	0.0	0.0	49.3	88.1	24.0
C5	3	40.46	48.0	0.0	0.2	51.2	80.2	23.8
C6	12	390.22	344.8	122.9	211.5	213.7	32.1	17.9
C7	29	175.27	212.3	31.9	58.7	92.5	9.0	24.8
C8	29	129.33	173.4	15.4	28.1	76.4	9.8	26.8
C9	23	262.98	276.2	66.2	123.5	136.2	14.1	22.7
C10	29	169.48	207.4	29.6	54.7	89.0	10.1	24.9
C11	11	391.42	344.3	123.6	224.5	226.1	22.8	17.6
C12	24	342.03	320.8	101.3	187.8	193.1	6.9	18.7
C13	16	393.48	346.3	124.4	224.5	215.7	15.2	17.8
C14	20	315.25	307.0	89.0	161.3	167.8	7.8	21.0
C15	28	194.99	228.4	39.0	72.9	101.0	11.2	24.5
C16	25	252.77	269.7	62.0	115.9	68.6	9.3	23.1

sidering the data in Table 3, the C4 and C5 samples had high ash content of about 88% and 80%, respectively. These two samples were obtained in operating conditions of 950 °C and holding time longer than 60 minutes. These relatively high values of ash content are due to pore destructions. It can be stated that all of the carbon in the sample had reacted with CO_2 in these conditions, and had been consumed during the reaction, in which brought about a minimum yield percentage (3%) for the experiments C4 and C5. The least SSA, total pore volume, micropore volume, and micropore surface area are also ascribed to these two prototypes.

According to Table 2 and Table 3, there is a direct relationship between specific surface area (derived from BET) and the other textural properties of activated carbon. The total pore volume increased along with the increasing micropore volume due to favorable activation conditions. The formation of micropores caused the number of pores to multiply, the surface area of micropores to become larger, and the SSA to rise. In addition, for all the samples, the amounts of micropore volume obtained through the DR method

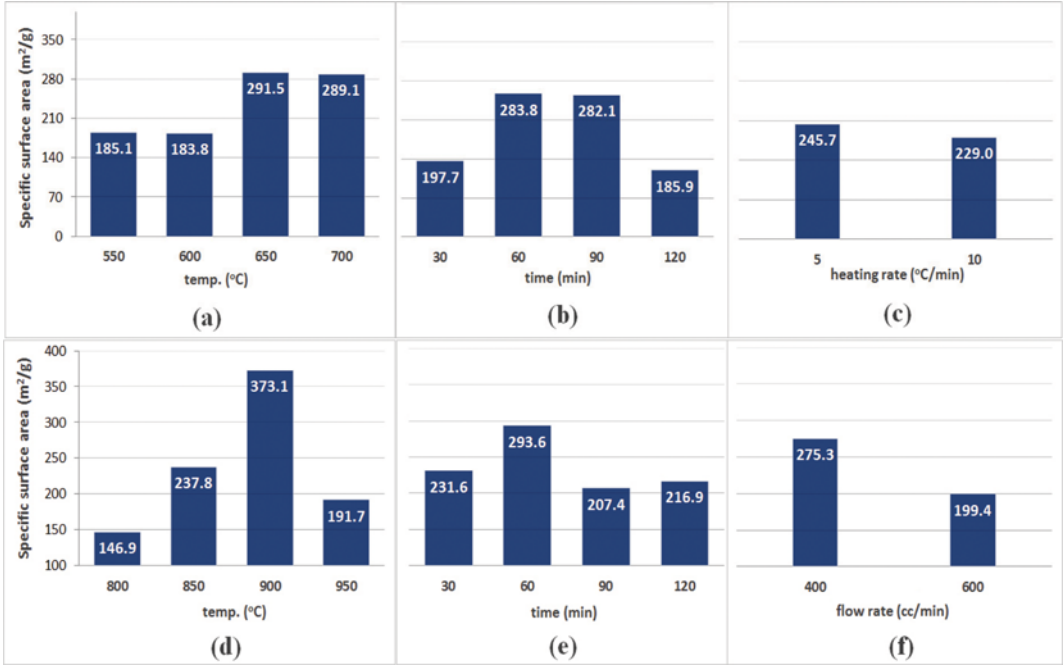

Fig. 2. Effect of different levels of operating parameters on the response (SSA). (a) Carbonization temperature, (b) carbonization time, (c) heating rate, (d) activation temperature, (e) activation time, (f) CO_2 flow rate.

Table 4. Analysis of variance (ANOVA) of main parameters involved in the production of activated carbon from scrap tires

Parameter	Degree of freedom (DOF)	Sums of squares (SS)	Variance (V)	*F*-ratio	*F*-value (1%)	Percent (%)
Carbonization temp.	3	44842.67	14947.56	353.58	540	18.99
Carbonization time	3	33513.68	11171.23	264.25	540	14.18
Heating rate	1	1114.38	1114.38	26.36	405	0.46
Activation temp.	3	114839.62	38279.87	905.50	540	48.72
Activation time	3	18036.51	6012.17	142.22	540	7.61
CO_2 flow rate	1	23045.51	23045.51	545.14	405	9.77
Error/Others	1	42.27	42.27	-		0.27

were greater than those obtained through *t*-method.

Maximum SSA, total pore volume and micropore volume found for sample C13 were 393 m^2/g, 0.346 cc/g, and 0.124 cc/g, respectively. Other samples such as C11, C6 and C3 also had high SSA values above 350 m^2/g. These results reveal that the SSA values for all the samples were around 390 m^2/g even though the preparation conditions were different. However, there can be optimum operating conditions that will maximize SSA.

The average pore radii for all samples were between 18-26 Angstrom. Pore radius had a direct correlation with the SSA, total pore volume and micropore volume. For the samples featuring high total pore volume and micropore volume, the average pore size decreased. In other words, when the micro-porosity was high, the pore size diminished significantly.

1. Effect of Parameters

To investigate the effect of a single parameter on SSA, the average results for each level were calculated and are shown in Fig. 2. The overall average SSA of all the samples was 237.4 m^2/g.

As can be seen in Fig. 2(a), the maximum SSA was around 290 m^2/g at higher carbonization temperatures near 650 °C (level 3) and 700 °C (level 4). When SSA increased at higher temperatures, it caused oils and non-carbonic elements to separate from the tire structure, and allowed pore expansion to take place. Fig. 2(b) suggests a similar trend for SSA values with increasing carbonization time, except that the SSA decreased after 90 min (level 3). Therefore, there is an optimum carbonization time after which the holding time will have a negative impact on SSA.

According to Fig. 2(c), elevating the heating rate from 5 °C/min (level 1) to 10 °C/min (level 2) did not significantly affect the SSA. The small drop in SSA, when the heating rate increased to 10 °C/min, means that the rate of carbonization reaction went up, and the materials remained in the reactor for a shorter time. Hence, the number of micropores and mesopores formed in the carbon structure were somewhat fewer at 10 °C/min.

Fig. 2(d) implies that the activation temperature was the parameter able to change the SSA the most, with a steep slope from level 1 (800 °C) to level 4 (950 °C). The SSA grew sharply up to level 3 (900 °C) due to the pore structure development and the formation of new micropores. The pore walls started to crumble after level 3 at temperatures higher than 900 °C. Consequently, the micropores merged to form a newly unfavorable configuration of mesopores and macropores, giving rise to a decline in the SSA.

The correlation of SSA with activation time is roughly similar to that with activation temperature. At first, SSA increased from level 1 (30 min) up to level 2 (60 min), and then decreased after that time (Fig. 2(e)).

Fig. 2(f) shows the effect of CO_2 flow rate on the SSA. Owing to the increased reaction rate and gasification at level 2 (600 cc/min of CO_2 flow rate), in which more pore walls collapsed compared to level 1 (400 cc/min), some micropores converted to mesopores and macropores, causing the SSA to diminish accordingly.

An analysis of variance (ANOVA) was implemented to find those process parameters that were statistically consequential in activated carbon production along with their confidence level and interactions. The ANOVA was based on degree of freedom (DOF), sums of squares (ss), variance and *F*-test (Fisher test). The ANOVA results are detailed in Table 4. With respect to these results, activation temperature is the most contributing parameter, and has the greatest influence (about 49%). Other notable parameters are carbonization temperature and carbonization time with about 19% and 14% influence, respectively. The effect of heating rate was near zero percent, which means that raising the heating rate from 5 to 10 °C/min had practically no impact on the SSA. The associated error in ANOVA is slight and negligible, confirming that there is a good agreement between the predicted and the experimental values, and the interactive effects of other parameters are indeed imperceptible.

The analysis of *F*-value is a test that points out the statistical significance of a parameter affecting the response. Through this analysis, the *F*-ratio of a parameter is compared to an *F*-value with a specific confidence level based on the degree of freedom. It means that for a confidence level of 99% (*F*-1%), if the *F*-ratio of the parameter is bigger than *F*-1%, then the parameter is statistically significant with a 99% confidence level [45]. On this basis, the activation temperature and CO_2 flow rate whose *F*-ratios (950.5 and 545.14) were bigger than *F*-1% (540 and 405, respectively), could be considered statistically significant with a 99% confidence level.

2. Optimization of Specific Surface Area

To maximize SSA, the operating parameters were optimized adopting Taguchi method, and the following optimal conditions were obtained:

- Carbonization temperature: 650 °C
- Carbonization time: 60 min
- Heating rate: 5 °C/min
- Activation temperature: 900 °C
- Activation time: 60 min
- CO_2 flow rate: 400 cc/min

Taguchi design anticipated an SSA of 465.2 m^2/g at optimum conditions. So, a confirmation test was carried out to examine the

Table 5. Elemental analysis of raw material (scrap tires) and optimized activated carbon

Sample	Carbon (%)	Hydrogen (%)	Nitrogen (%)	Sulphur (%)
Scrap tire	73.50	4.15	0.15	20.12
Optimized activated carbon (OAC)	78.63	4.20	0.07	14.91

optimum conditions. The confirmation experiment was repeated and the optimize sample was analyzed. Interestingly, the SSA value of activated carbon obtained at optimum conditions was 437.1 m^2/g. The almost 6% difference between the design's prediction and the value found in practice through real optimum conditions seems reasonable and relatively low. The difference could be attributed to uncontrollable environmental conditions such as temperature fluctuations and noise factors. The sample obtained at optimum conditions was named optimized activated carbon (OAC) and was comprehensively analyzed.

In our previous research [54], the process yield and iodine number were optimized in activated carbon production process. The optimum conditions for the process yield functioning as response were as follows:

Carbonization temperature: 700 °C, Carbonization time: 60 min, activation temperature: 800 °C, activation time: 30 min, and CO_2 flow rate: 400 cc/min.

The optimum conditions obtained for iodine number were in this way:

Carbonization temperature: 700 °C, Carbonization time: 60 min, activation temperature: 900 °C, activation time: 60 min and CO_2 flow rate: 400 cc/min.

Based on these results, it can be concluded that iodine number and SSA responses are analogous, and the optimum conditions for both are nearly the same. The comparison of optimum conditions for the process yield with those for SSA (or iodine number) reveals that the carbonization conditions were the same, but the maximum yield was reached at different activation conditions, *i.e.,* 800 °C (which is the lowest temperature) and an activation duration of 30 min.

3. The Characteristics of Optimized Activated Carbon

Making a comparison between CHNS elemental analysis for the raw scrap tire and the OAC (Table 5) reveals that the carbon content increased (on account of carbonization and activation processes) and the amount of sulfur dropped. This may be due to separation of some compounds, *e.g.*, SO_x, H_2S and other sulfuric compounds, via the pyrolysis of scrap tires. Some sulfur content was removed from the tire structure during the pyrolysis (carbonization) process, and thus the amount of sulfur decreased. Meanwhile, the content of hydrogen and nitrogen did not change markedly.

Physical and chemical characteristics of the optimized sample are detailed in Table 6.

Table 6. Characteristics of activated carbon prepared at optimum conditions (OAC)

Characteristic	Value
Specific surface area (BET)	437.1 [m^2/g]
Total pore volume (*t*-method)	353.6 [$\times 10^{-3}$ cc/g]
Micropore volume (*t*-method)	112.3 [$\times 10^{-3}$ cc/g]
Micropore surface area (*t*-method)	130.3 [m^2/g]
Average pore radius	18.7 [A]
Iodine number	404.7 [mg I_2/g]
Yield	13.2%
Bulk density	0.20 [g/ml]
pH	10.2
Conductivity	395 [μs/cm]
Ash content	13.9%

The ash content was about 14% for OAC, which is an acceptable percentage, bearing in mind that no ash reduction treatment such as demineralization was administered.

The pH of OAC was about 10. This pH value represents the basic nature of activated carbon which can be ascribed to the formation of functional groups during its reaction with CO_2. This property makes OAC unsuitable for the removal of acidic compounds such as acid dyes.

The OAC exhibited a relatively high value of conductivity, which may come from the relatively high ash content and the subsequent high amount of leachable minerals, or a large number of functional groups on the activated carbon.

Tables 6 and 7 indicate that these properties are comparable with the results of other studies. Gonzalez et al. were able to achieve a surface area of 496 m^2/g at 850 °C, 3 hr activation time, and with 600 cc/min of CO_2 flow rate. The high carbonization temperature and long activation time resulted in a rather large SSA [55]. Suuberg et al. ground and powdered the char (320-420 μm) after the pyrolysis, and then ran a second pyrolysis at 900 °C for 1 hr before activation. They obtained a surface area of 650 m^2/g with adjusting the carbon dioxide partial pressure at 4.80 kPa, and exploiting helium as the CO_2 carrier gas. These conditions helped to gain a

Table 7. Brief summary of other studies conducted on activated carbon preparation from tire wastes by CO_2

Reference	Carbonization conditions	Activation conditions	CO_2 flow rate [cc/min]	Surface area (BET) [m^2/g]
Gonzalez et al. [55]	800 °C, 1 h	850 °C, 3 h	600	496
Suuberg et al. [56]	700 °C, 5 min	850 °C, 1 h	220	650
Betancur et al. [14]	-	900 °C, 3 h	150	414.5
Choi et al. [57]	500 °C, 2 h	950 °C, 3 h	5 NL/min	437
Acevedo et al. [19]	850 °C	850 °C	250	496

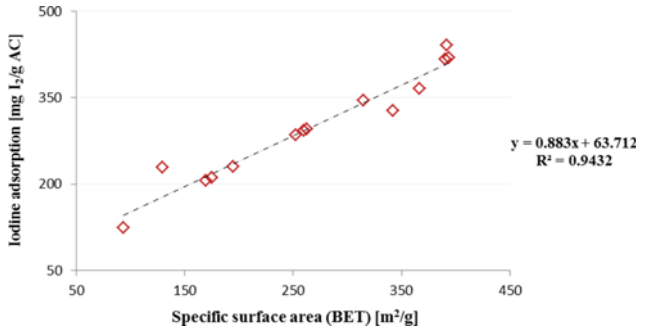

Fig. 3. The relation between SSA and Iodine number of activated carbon samples.

high surface area [56]. Betancur et al. manufactured activated carbon from scrap tires through direct CO_2 activation (150 ml/min) at 900 °C with 3 hr activation time without any carbonization or pyrolysis, and reached a surface area of 414.5 m^2/g at those conditions [14]. Choi et al. optimized their activated carbon with a 437 m^2/g BET surface area, performing activation at 950 °C for 3 hr [57]. However, interestingly, we were able to achieve nearly the same SSA by running activation at a lower activation temperature (900 °C) and shorter time (1 hr). Acevedo et al. obtained a 496 m^2/g surface area through activation with a CO_2 flow rate of 250 cc/min at 850 °C. The activation time was long enough (until the burn-off reached about 65%) to produce an activated carbon with a convincingly high SSA [19].

The correlation between SSA and the iodine adsorption capacity of the produced activated carbon is demonstrated in Fig. 3. There is a direct relationship between the Iodine number and the SSA, and any increase in SSA will subsequently boost the accessible volume of the activated carbon pores that will be filled by Iodine molecules. A linear regression was constructed for the data points, which exhibits a good convergence with R^2=0.94. The slope of the line was near 1, implying that the iodine number was approximately equal to SSA. Therefore, it is a fairly convenient estimation tool for calculating one of the responses (SSA or iodine number) using the corresponding values of another one.

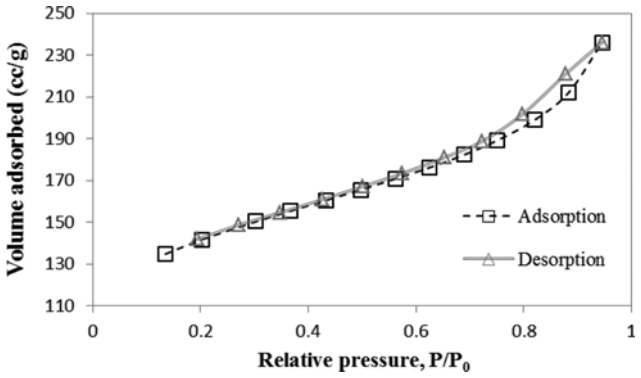

Fig. 5. Adsorption-desorption isotherm of SSA optimized activated carbon (OAC) at 77 K.

Fig. 4 illustrates the SEM images from a sample of scrap tire rubber with 10000× magnification zoom, and OAC with two different magnification zooms of 5000× and 10000×. As can be seen in Fig. 4(a), the scrap tire sample was fully plain without any void fractions. However, it is obvious from Fig. 4(b) and (c) that the cavities and rough textures were clearly formed when the organic compounds in the tire were released at high temperatures during the reaction with CO_2. There are different kinds of pores in the activated carbon, including some micropores and macropores, but mostly mesopores; so, the activated carbon is considered mesoporous as the BET analysis has already shown.

The nitrogen adsorption-desorption isotherm for OAC (at 77 K) is presented in Fig. 5. Based on IUPAC classification, the isotherm is type IV, which reflects the fact that most of the pores are mesopores rather than micropores. An inflection can be observed, at the first three adsorption points due to the coverage of the first adsorbed monolayer. Since capillary condensation has occurred in the mesopores, a hysteresis of adsorption-desorption loop has been created. Capillary condensation takes place as a consequence of the meniscus formation of the liquefied adsorbate. The capillary condensation and evaporation do not often happen at the same pressure, and this leads to H3 type hysteresis phenomenon, which is an intermedi-

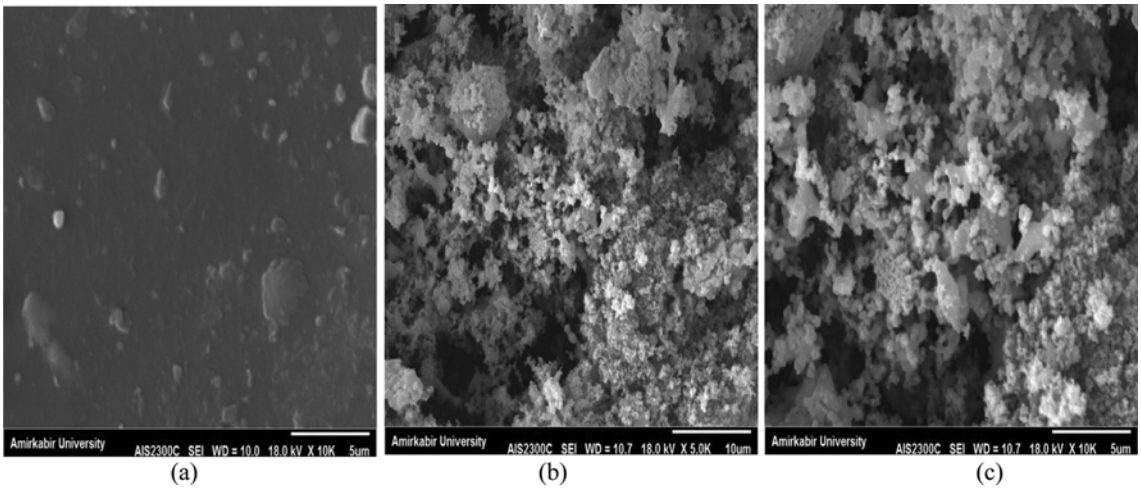

Fig. 4. SEM pictures of (a) scrap tire (b) optimized activated carbon (OAC) with 5 k zoom and (c) 10 k zoom.

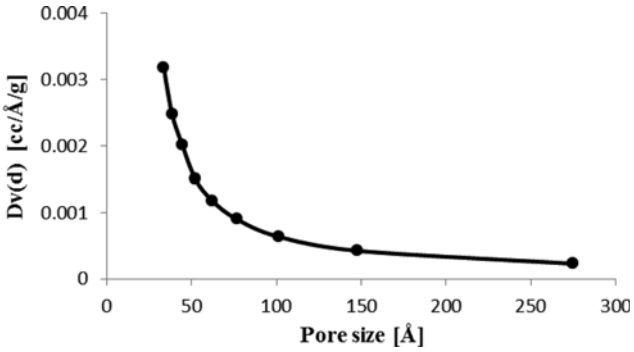

Fig. 6. The Barrett, Joyner, and Halenda (BJH) adsorption pore size distribution for SSA optimized activated carbon (OAC).

ate state of SSA with the two basic types of H1 and H4 hysteresis. The H3 type hysteresis represents the pores that are mostly slit-shaped, and the activated carbon that is made up of plate-like particles [46].

The pore size distribution contains information on the amount of pore volume available to adsorbate molecules of a given shape and size. Based on IUPAC classification [58], adsorbent pores are divided into three groups of micropores (d<20 Å), mesopores (20< d<500 Å), and macropores (d>500 Å). Fig. 6 shows the Barrett, Joyner and Halenda (BJH) adsorption pore size distribution of the OAC. The plot confirms that the activated carbon is nearly mesoporous with the majority of pore sizes between 30 and 50 Å, and an average pore diameter of 37.34 Å. The pore volume distribution gradually decreases with increasing pore size, and shifts to macroporosity.

The changes in FTIR spectra of scrap tire samples and OAC are demonstrated in Fig. 7. Apparently, scrap tire has many banded functional groups like OH (3,432.65 cm^{-1}), C-O (1,035.17 cm^{-1}), S=O (1,444.11 cm^{-1}) and aromatic (874.77 cm^{-1}) or aliphatic groups. The peak at 479 cm^{-1} represents the groups of S-S, and the peak at 796-801 cm^{-1} refers to the stretching aromatic compounds (C-H). The strong and broad adsorption peak at 1,111 cm^{-1} corresponds to the stretching of the C-O oxygenated functional groups, and it suggests the presence of carboxylic acid, ether, and ether functional groups in activated carbon. The symmetric band found at 1,384 cm^{-1} indicates the groups of -CH_3, and there is a possibility for the

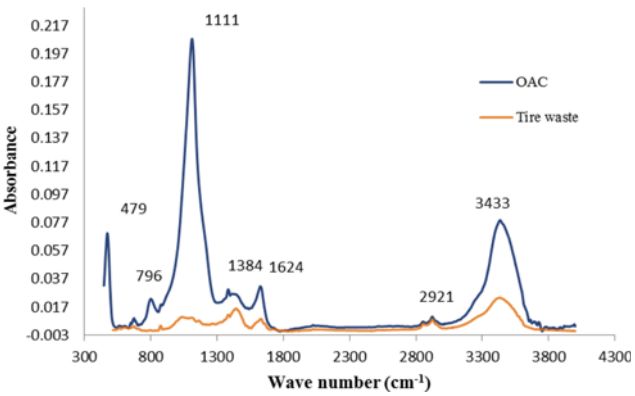

Fig. 7. The FTIR analysis of scraptire raw material and OAC.

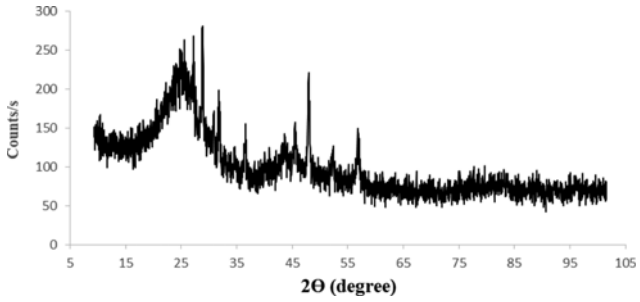

Fig. 8. The X-ray diffraction (XRD) analysis of optimized activated carbon.

presence of S=O groups at this peak as well. The other functional groups are C=N stretch vibration at 1,624 cm^{-1}, and aliphatic -CH stretching at 2,921 cm^{-1}. Finally, another noticeable shoulder around 3,433 cm^{-1} specifies the OH groups, which have formed during carbonization and activation processes [18,59].

The X-ray diffraction (XRD) analysis was done on the OAC sample and the results are shown in Fig. 8. The diagram exhibits two main peaks at around 2θ=28° (d=3.09 Å) and 47° (d=1.89 Å). It can be deduced from these peaks that the activated carbon is most likely amorphous and does not represent a crystalline structure.

CONCLUSIONS

Activated carbon was produced from scrap tires, and the effect of operating parameters on the specific surface area (SSA) was investigated. The entire process is comprised of two steps of carbonization and activation by carbon dioxide as the activating agent. The experiments were based on Taguchi experimental design. The analysis of variance made clear that the leading factor was the activation temperature with about 49% effect on the SSA. The optimum conditions obtained for the maximum SSA were: carbonization temperature=650 °C, carbonization time=60 min, heating rate=5 °C/min, activation temperature=900 °C, activation time=60 min and CO_2 flow rate=400 cc/min. Also, the activated carbon SSA at optimum conditions was about 437 m^2/g. The prepared activated carbon was a mesoporous adsorbent with a predominantly amorphous structure, numerous oxygen functional groups, high electric conductivity and moderate ash content. The produced sample had good iodine adsorption capacity (proportional to the SSA) as well, and could be taken advantage of in industrial sorption processes aimed at elimination of organic compounds.

ACKNOWLEDGEMENT

The authors gratefully acknowledge that this project was financially supported by a research grant (research project 1/1/441) from Danesh-e Tandorosti Institute. The authors sincerely thank Mr. Amir Hassan Faramarzi for his contributions in building the apparatus and assembling the experimental system.

REFERENCES

1. J. D. Martínez, N. Puy, R. Murillo, T. García, M. V. Navarro and

A. M. Mastral, *Renew. Sust. Energy Rev.*, **23**, 179 (2013).
2. Managing end-of-life-tires-full report, World Business Council for Sustainable Development (November 2008).
3. P. Parthasarathy, H. S. Choi, H. C. Park, J. G. Hwang, H. S. Yoo, B.-K. Lee and M. Upadhyay, *Korean J. Chem. Eng.*, **33**, 2268 (2016).
4. O. Onay and H. Koca, *Fuel*, **150**, 169 (2015).
5. E. Commission, Landfill of waste directive, council directive 1999/31/ec, European Commission, Brussels (1999).
6. P. Pipilikaki, M. Katsioti, D. Papageorgiou, D. Fragoulis and E. Chaniotakis, *Cement Concrete Res.*, **27**, 843 (2005).
7. E. L. Mui, D. C. Ko and G. McKay, *Carbon*, **42**, 2789 (2004).
8. J. A. Conesa, A. Gálvez, F. Mateos, I. Martín-Gullón and R. I. Fon, *J. Hazard. Mater.*, **158**, 585 (2008).
9. F. Carrasco, Y. Gningue and M. Heitz, *Environ. Technol.*, **19**, 461 (1998).
10. A. Benazzouk, O. Douzane, T. Langlet, K. Mezreb, J. M. Roucoult and M. Quéneudec, *Cement Concrete Comp.*, **29**, 732 (2007).
11. M. Arabani, S. M. Mirabdolazimi and A. R. Sasani, *Constr. Build. Mater.*, **24**, 1060 (2010).
12. F. J. Navarro, P. Partal, F. Rancisco, J. Martínez-Boza and C. Gallegos, *Polymer Testing*, **29**, 588 (2010).
13. A. Fernández, C. Barriocanal and R. Alvarez, *J. Hazard. Mater.*, **203**, 236 (2012).
14. M. Betancur, J. D. Martínez and R. Murillo, *J. Hazard. Mater.*, **168**, 882 (2009).
15. O. Chan, W. Cheung and G. McKay, *Carbon*, **49**, 4674 (2011).
16. A. Alsaleh and M. L. Sattler, *Curr. Sust./Renewe. Energy Rep.*, **1**, 129 (2014).
17. T. A. Saleh and V. K. Gupta, *Adv. Colloid Interface*, **211**, 93 (2014).
18. B. Acevedo and C. Barriocanal, *Fuel Process. Technol.*, **134**, 275 (2015).
19. B. Acevedo, C. Barriocanal, I. Lupul and G. Gryglewicz, *Fuel*, **151**, 83 (2015).
20. R. Acosta, C. Tavera, P. Gauthier-Maradei and D. Nabarlatz, *Int. J. Chem. React. Eng.*, **13**, 189 (2015).
21. M. Betancur, J. D. Martínez and R. Murillo, *J. Hazard. Mater.*, **168**, 882 (2009).
22. Y. Ngernyen, C. Tangsathitkulchai and M. Tangsathitkulchai, *Korean J. Chem. Eng.*, **23**, 1046 (2006).
23. G. Wu, T.-s. Jeong, C.-H. Won and L. Cui, *Korean J. Chem. Eng.*, **27**, 1476 (2010).
24. P. Parthasarathy and S. Narayanan, *Korean J. Chem. Eng.*, **32**, 2236 (2015).
25. H.-Y. Kang, S.-S. Park and Y.-S. Rim, *Korean J. Chem. Eng.*, **23**, 948 (2006).
26. J. M. Dias, M. Alvim-Ferraz, M. F. Almeida, J. Rivera-Utrilla and M. Sánchez-Polo, *J. Environ. Manage.*, **85**, 833 (2007).
27. C.-I. Su, Z.-L. Zeng, C.-C. Peng and C.-H. Lu, *Fiber. Polym.*, **13**, 21 (2012).
28. E. Ekrami, F. Dadashian and M. Soleimani, *Fiber. Polym.*, **15**, 1855 (2014).
29. A. Esfandiari, T. Kaghazchi and M. Soleimani, *J. Taiwan Inst. Chem. Eng.*, **43**, 631 (2012).
30. E. L. K. Mui, W. H. Cheung, M. Valix and G. McKay, *Micropor. Mesopor. Mater.*, **130**, 287 (2010).
31. B. G. V. K. Gupta, A. Rastogi, S. Agarwal and A. Nayak, *J. Hazard. Mater.*, **186**, 891 (2001).
32. G. S. Miguel, G. D. Fowler, M. Dall'Orso and C. J. Sollars, *J. Chem. Technol. Biot.*, **77**, 1 (2002).
33. R. Helleur, N. Popovic, M. Ikura, M. Stanciulescu and D. Liu, *J. Anal. Appl. Pyrol.*, **58**, 813 (2001).
34. M. Alexandre-Franco, C. Fernández-González, A. Macías-García and V. Gómez-Serrano, *Adsorption*, **14**, 591 (2008).
35. G. Skodras, I. Diamantopoulou, A. Zabaniotou, G. Stavropoulos and G. Sakellaropoulos, *Fuel Process. Technol.*, **88**, 749 (2007).
36. L. Li, S. Liu and T. Zhu, Tan Zhu, *J. Environ. Sci.*, **22**, 1273 (2010).
37. A. Belgacem, R. Rebiai, H. Hadoun, S. Khemaissia and M. Belmedani, *Environ. Sci. Pollut. R.*, **21**, 684 (2014).
38. V. Gupta, B. Gupta, A. Rastogi, S. Agarwal and A. Nayak, *Water Res.*, **45**, 4047 (2011).
39. M. Hofman and R. Pietrzak, *Chem. Eng. J.*, **170**, 202 (2011).
40. T. Brady, M. Rostam-Abadi and M. Rood, *Gas Sep. Purif.*, **10**, 97 (1996).
41. I. Ali, *Sep. Purif. Rev.*, **43**, 175 (2014).
42. I. Ali, *Sep. Purif. Rev.*, **39**, 95 (2010).
43. I. Ali, M. Asim and T. A. Khan, *J. Environ. Manage.*, **113**, 170 (2012).
44. I. Ali, *Chem. Rev.*, **112**, 5073 (2012).
45. D. C. Montgomery, *Design and analysis of experiments*, John Wiley & Sons (2008).
46. R. C. Bansal and M. Goyal, *Activated carbon adsorption*, CRC Press (2010).
47. S. Brunauer, P. H. Emmett and E. Teller, *J. Am. Chem. Soc.*, **60**, 309 (1938).
48. P. Barrett, L. Joyner and P. P. Halenda, *J. Am. Chem. Soc.*, **73**, 373 (1951).
49. C. Saka, *J. Anal. Appl. Pyrol.*, **95**, 21 (2012).
50. ASTM, *Standard test method for apparent density of activated carbon*, *D2854-96*, The American Society for Testing and Materials (2004).
51. ASTM, *Standard test method for pH of activated carbon*, The American Society for Testing and Materials (2000).
52. ASTM, *Standard test method for total ash content of activated carbon*, The American Society for Testing and Materials (2004).
53. M. Ahmedna, W. Marshall and R. Rao, *Bioresour. Technol.*, **71**, 113 (2000).
54. Z. Loloie, M. Soleimani and M. Mozaffarian, Optimisation of physical activation process for activated carbon production from tyre wastes, *Int. J. of Global Warm.*, Inderscience Enterprises Ltd. (2015).
55. J. F. González, J. M. Encinar, C. M. González-García, E. Sabio, A. Ramiro, J. L. Canito and J. Gañán, *Appl. Surf. Sci.*, **252**, 5999 (2006).
56. E. M. Suuberg and I. Aarna, *Carbon*, **45**, 1719 (2007).
57. G.-G. Choi, S.-H. Jung, S.-J. Oh and J.-S. Kim, *Fuel Process. Technol.*, **123**, 57 (2014).
58. K. S. Sing, *Pure Appl. Chem.*, **57**, 603 (1985).
59. J. Zhu, H. Liang, J. Fang, J. Zhu and B. Shi, *Clean Soil Air Water*, **39**, 557 (2011).